ANU-P/954
December 1986

TRANSIENT-FIELD STRENGTH MEASUREMENTS FOR ^{52}Cr TRAVERSING Fe HOSTS AT HIGH VELOCITY AND POLARIZATION TRANSFER MECHANISMS

A.E. Stuchbery, C.E. Doran, A.P. Byrne,

H.H. Bolotin and G.D. Dracoulis

Department of Nuclear Physics
Australian National University

and
School of Physics, University of Melbourne

ANU-P/954
December 1986

Accepted for publication in Hyperfine Interactions

TRANSIENT-FIELD STRENGTH MEASUREMENTS FOR ^{52}Cr TRAVERSING Fe HOSTS AT HIGH VELOCITY AND POLARIZATION TRANSFER MECHANISMS.

A. E. Stuchbery
Department of Nuclear Physics,
Research School of Physical Sciences,
Australian National University.
GPO Box 4, Canberra, 2601 A.C.T.
Austalia.

and

School of Physics,
University of Melbourne,
Parkville Vic. 3052.
Australia.

and

C.E. Doran, A.P. Byrne† and H.H. Bolotin,
School of Physics,
University of Melbourne,
Parkville Vic. 3052.
Australia.

and

G.D. Dracoulis,
Department of Nuclear Physics,
Research School of Physical Sciences,
Australian National University,
GPO Box 4, Canberra 2601 A.C.T.
Australia.

† National Research Fellow

Abstract

Transient-field strengths were measured for ^{52}Cr ions traversing polarized Fe hosts at velocities up to $12v_o$ ($v_o = c/137$ = Bohr velocity). The results are compared with predictions of various transient field parametrizations and discussed in terms of possible mechanisms by which polarization might be transferred from the Fe host to inner vacancies of the moving Cr ions. The g-factor of the first 2^+ state of ^{52}Cr was also measured by the transient field technique and found to be in accord with shell-model calculations.

Introduction

While the transient hyperfine magnetic field (TF) is being successfully exploited to measure magnetic moments of short-lived nuclear states, the mechanisms leading to the TF phenomenon remain, on the whole, only qualitatively understood. Although, it is well established that the large transient magnetic field produced at the nucleus of an ion traversing a polarized ferromagnetic medium arises from unpaired electrons in s orbitals of the recoiling ion which have a net polarization transferred from the host, little is understood about how the polarization of the outer electron orbitals of the ferromagnetic host is transferred to low-lying vacancies of the moving ion.

The present paper reports measurements of the g-factor of the 2_1^+ state of ^{52}Cr and of TF strengths for ^{52}Cr ions traversing Fe hosts at velocities up to $12v_o$ (v_o = c/137 = Bohr velocity). This work was motivated after consideration of possible polarization-transfer mechanisms (see discussion section below). One particular model suggests that the TF strength for <u>all</u> ions traversing Fe hosts, which generally increases with velocity, might begin to level off (and then diminish with increasing ion velocity) at around 7 to $8v_o$. The Chalk River group has already reported measurements for rare-earth ions traversing Fe which do display a diminution of the TF strength for ion-velocities above $8v_o$ [1]. Experiments were undertaken to begin to test this prediction for intermediate mass ions and thereby to more critically examine the alternative mechanisms by which polarization transfer proceeds.

2. Experimental Design

Nuclei of mass number around 50 can be Coulomb excited and made to recoil at large velocities (~$12v_o$) by bombardment with heavy ions, e.g.

^{81}Br at energies of ~2.5 MeV/nucleon. However, to obtain a reasonably high degree of nuclear alignment (leading to anisotropic de-excitation γ-ray angular distributions) and to constrain the recoil angles at which ions enter the host foil, the forward scattered target ions must be detected at angles close to the beam direction. The reaction geometry of such an implanted perturbed angular correlation (IMPAC) measurement then corresponds, in the centre of mass frame, to one in which backscattered projectiles are detected in coincidence with de-excitation γ rays. However for forward scattered target ions, such a coincidence requirement effectively limits suitable probe states to those with lifetimes ~ 1 ps in order that (a) the γ-ray decay takes place very close to the target, obviating the need for 'extended source' corrections to the observed (perturbed) angular distributions, and (b) decays take place before appreciable vacuum deorientation occurs. In view of this restriction, the 1.434 MeV 2_1^+ state of ^{52}Cr (τ = 1.0 ps) was chosen as the probe. It has an added advantage, due to its predominantly $(\pi f_{7/2})^4$ configuration, of having a relatively large g-factor (empirical shell model value g = 1.456 [2] in accord with measured value reported below).

3 Experimental Procedures

Beams of 220, 230, 240 MeV ^{81}Br ions from the ANU 14UD Pelletron accelerator were used to excite targets of natural Cr (84% ^{52}Cr). Two targets were employed. Target I consisted of 1.04 mg. cm^{-2} of natural Cr evaporated onto an annealed, 10.7 μm-thick Fe foil. Target II had 0.86 mg.cm^{-2} of natural Cr evaporated onto an annealed, 5.7 μm-thick Fe foil with a layer of natural Cu, 1.3 mg.cm^{-2} thick, evaporated on the downstream side. A further 5 μm thick Cu foil was placed on the downstream side of this target to stop the ^{81}Br beam while allowing the

^{52}Cr ions to emerge from the target layers.

De-excitation γ rays were recorded in coincidence with forward recoiling ^{52}Cr ions detected in an annular silicon surface barrier detector which subtended angles between 7° and 17° in the lab frame (corresponding, in the CM frame, to backscattered ^{81}Br angles of 135° to 162°).

To confirm that vacuum deorientation of the 2_1^+ -state was negligible, target II was bombarded by beams of 240 MeV ^{81}Br and the ^{52}Cr γ-ray angular correlation was measured with one HP Ge detector placed successively at 45°, 55° and 65° to the beam direction while another fixed at -65° served as a monitor. (Due to physical constraints only angles between 45° and 65° could be sampled.) The distance between the target and the face of the γ-ray detector was 6.0 cm.

Transient field precessions were measured for both targets. Two 7.62 cm x 7.62 cm NaI detectors were placed 9.7 cm from the target at ± 65° to the beam axis and two HP Ge detectors placed 6.0 cm from the target at ± 115°. A polarizing field of 0.04 Tesla was applied to the targets and reversed frequently in the direction normal to the reaction plane. Soft iron cones shielded the incoming beam ions and outgoing Cr ions from the stray magnetic field of the electromagnet rendering 'beam bending' effects negligible.

To measure the g-factor of the 2_1^+ state of ^{52}Cr, target II (5.7 μm Fe foil) was also bombarded by 36 MeV ^{18}O ions from the ANU 14UD pelletron accelerator. The precessions of the 2_1^+ states of ^{52}Cr and ^{56}Fe were measured at low velocity in the conventional backscattered-projectile geometry (backscattered ^{18}O ions detected in the angular range 146° - 166)°.

Full saturation of the Fe foils in situ was confirmed by measurement of the OsFe static-field interaction following implantation of ^{188,190,192}Os ions into the Fe foils used. After the Cr precession measurements, ~1 mg.cm^{-2} of natural osmium was electroplated onto the rear of target I. As it was not practicable to plate Os on the back of target II, a piece of the annealed 5.7 μm Fe foil from which target II was prepared was used. The first 2^+ states of ^{188,190,192}Os were excited by 90 MeV ^{35}Cl beams and the static-field precessions measured (with the detector geometry as employed for the TF measurement with backscattered ^{16}O ions).

For each bombardment the required particle-γ angular correlations were calculated using statistical tensors obtained from the Winther-de Boer code [3]; finite solid-angle correction factors for the HP Ge detectors were calculated in a manner similar to Krane [4], while those for the NaI detectors were interpolated from tables [5]. In all cases, population of states higher than the 2_1^+ state in ^{52}Cr and ^{56}Fe was negligible. Our experience [6,7] is that particle-γ angular correlations following Coulomb excitation may be calculated reliably in such cases.

In all experimental runs coincidences were recorded on magnetic tape in the event-by-event mode for later off-line analysis.

4 Results

4.1 ^{52}Cr- γ-ray Angular Correlation

The γ-ray angular correlation of the ^{52}Cr $2_1^+ - 0_1^+$ decay, measured in coincidence with forward scattered ^{52}Cr ions following excitation with 240 MeV ^{81}Br beams is shown in fig. 1. The calculated curve (full line) is in excellent accord with the measured points, confirming that the 2_1^+ -

state decay takes place before any significant vacuum deorientation occurs. (For a mean life of 1 ps a typical vacuum deorientation time of $\tau_2 \sim 60$ ps, observed for ^{48}Ti and ^{56}Fe ions [8], in the Abragam-Pound theory [9] yields an integral attenuation coefficient of $G_2(\infty) \simeq 0.98$.) The coincidence particle and γ-ray spectra obtained at 45° to the beam are displayed in figs. 2 and 3, respectively.

4.2 Precession Measurements for ^{52}Cr and ^{56}Fe

Results of the precession measurements for the first excited state of ^{52}Cr following ^{16}O and ^{81}Br bombardments and of ^{56}Fe following ^{16}O bombardment are summarized in table 1. Figure 4 shows a spectrum of ^{16}O ions backscattered from target II in coincidence with γ-rays. The digital gates set to select beam ions scattered from the Cr and Fe layers of the target are marked. Note that the middle gate region includes backscattering from both the downstream side of the Cr layer and from the Fe layer. As evident in table 1, ^{52}Cr precessions were measured separately for each region. Figure 5 shows an HP Ge spectrum obtained at 65° to the beam direction in concidence with ^{16}O ions (beam energy 36 MeV) backscattered from the front of the Cr target layer.

4.3 Static Field Precession Measurements for Os in Fe

Static field strengths for Os<u>Fe</u> inferred from the present precession measurements for 5.7 μm- and 10.7 μm- thick Fe host foils (using previously measured g-factors [7]) are displayed in table 2. Analysis of these data followed the procedure outlined in ref. [7]. It is apparent from table 2 that the most precisely determined field strengths (i.e. for ^{192}Os) are, for both foils, in good accord with the field strength of 109.343±0.065 T determined by the NMR technique [10], while the average

for ^{188,190,192}Os together is also in accord with this value. This agreement justifies the assumption in the following analysis that the Fe foils were fully saturated during the ^{52}Cr, ^{56}Fe precession measurements.

5 Analysis

5.1 The ^{52}Cr 2_1^+ - state g-factor

The g-factor of the 2_1^+ state of ^{52}Cr has not been measured previously, yet shell model calculations of gyromagnetic ratios of 2_1^+ states in the $f_{7/2}$ shell are quite reliable (see e.g. refs [11,12]). In particular, the g-factor for the first excited state of ^{54}Fe, which in the shell model has an identical value to that of ^{52}Cr, has been measured to be $g(2_1^+; {}^{54}Fe) = 1.68 \pm 0.38$ [11] in accord with calculations [2]. Nevertheless, to be more certain about the g-factor of the 2_1^+ state of ^{52}Cr we present in this section measurements of precessions for ^{56}Fe<u>Fe</u> [$g(2_1^+; {}^{56}Fe)$ known] and ^{52}Cr<u>Fe</u>, which may be used to infer an experimental g-factor for the 2_1^+ state of ^{52}Cr.

It is well known [13,14] that a large discontinuity exists in the atomic-number dependence of the transient field for ion velocities $v<4v_0$ when the projectile 1s orbital crosses the 2p orbital of Fe (i.e. for Z~9). In earlier publications [15,16] we reported similar (but less pronounced) discontinuities occuring when the 3s- and 4s- orbitals of the projectile cross the 2p orbital of Fe (i.e. for Z~47 and Z~77, respectively) and pointed out [16,17] that a similar discontinuity might appear between $_{22}$Ti and $_{24}$Cr. Of import in the present context, we have noted [18] and presented evidence [18,19] that neighbouring ions of atomic number greater than that of the ion for which the orbital matching occurs have TF strengths at low velocity ($v<3.5v_0$) which are similar in form to

that of the ion for which the matching occurs. For example, in refs [18,19] evidence is presented that the TF strengths for $_{77}$Ir, $_{78}$Pt, $_{79}$Au, and $_{80}$Hg ions traversing Fe hosts are all diminished compared with those of $_{74}$W and $_{76}$Os ions and, to the precision of the available measurements, can be accommodated by a similar parametrization of the TF at low velocities. Therefore, if there is any diminution of the TF strength for Cr<u>Fe</u> at low velocities, the TF for Fe<u>Fe</u> is expected to behave similarly. For this reason we measure the g-factor of the first excited state of ^{52}Cr relative to that of the first excited state of ^{56}Fe. Precessions for these states were measured simultaneously following excitation with ^{16}O beams.

The observed total precession angle $\Delta\theta$ for a nuclear excited state (mean life τ, g-factor g) of an ion slowing to rest in a ferromagnetic host may be written as

$$\Delta\theta = -g \frac{\mu_N}{\hbar} \left[e^{-t_t/\tau} \int_{t_t}^{t_s} B_{tr} \; e^{-t/\tau} dt + e^{-t_s/\tau} B_{st} \tau \right] \quad (1)$$

where t_t is the average time for ions to traverse the target layer, t_s is the time at which ions come to rest in the host, B_{tr} is the TF strength, and B_{st} is the static field strength.

In the 'thin foil' TF technique, the ions traverse the ferromagnetic layer and come to rest in a non-magnetic backing layer. The static field contribution, B_{st}, in such measurements is then zero and t_s in eq (1) becomes the average time at which the ion emerges from the ferromagnetic foil layer.

While the static field contribution to the observed precession angle for the short-lived 2_1^+ state of ^{52}Cr (τ = 1.0 ps) is almost negligible in the present measurement, that for ^{56}Fe ($\tau(2_1^+)$ = 10 ps) is about half

the magnitude of, and opposite in sign to, the transient-field precession. To obtain a calibration of the TF strength for ^{56}Fe<u>Fe</u> in a 'thick foil' measurement, the observed total precession must be carefully corrected for the static field contribution. Tables 3A and 3B present a summary of the present 'thick foil' precession results for Fe<u>Fe</u> and Cr<u>Fe</u> and of both 'thick foil' and 'thir foil' results for Fe<u>Fe</u> reported by the Rutgers group [11,20,21]. Also in table 3A, the observed TF precessions for Fe<u>Fe</u> are compared with calculated precessions assuming a transient field strength given by

$$B_{tr} = 15.2\ Z^{1.1}\ (v/v_o)^{0.45}\ \text{Tesla}, \qquad (2)$$

which is 0.9 times the 'universal' TF parametrization proposed by Shu et al [21] (see also eq (6) below). It is apparent from table 3A that the present 'thick foil' precession is consistent with a TF strength given by eq (2), followed by precession due to a static field strength of -33.04±0.03T as obtained in radioactivity measurements [10,22]. In an earlier analysis of 'thick foil' Fe<u>Fe</u> precessions, Eberhardt and Dybdal [23] proposed a reduced static field strength of -21 T for implantation measurements, the reduction in static field strength being attributed to radiation damage. However, their analysis presupposed a TF strength <u>linearly</u> dependent on ion velocity. With the exception of the two lowest velocity precessions (Fe ions excited and recoiled by ~ 3 to 5 MeV protons [24]), the data included in their fit are better described by the non-linear TF given in eq (2) followed by the full static-field contribution.

While the separation of transient- and static-field contributions for low velocity Fe ions in Fe may remain somewhat ambiguous, the results summarized in table 3A demonstrate that our measurement is in accord with

those of other workers and, more importantly, that eq (2) is consistent with the 'thin foil' TF strengths for Fe<u>Fe</u> meausred by the Rutgers group at ion velocities above $4v_o$ where the field-strengths for Fe and Cr are expected to be similar, irrespective of any low-velocity disparity. Using eq (2), then, to define the TF for Cr<u>Fe</u>, and applying a small correction for the static field precession of Cr<u>Fe</u> (B_{st}(Cr<u>Fe</u>) = -6.66±0.04T[10]), the present low-velocity precession data for ^{52}Cr yield the g-factor for the 2_1^+ state: g=+1.50±0.25 (see table 3B). The quoted error incorporates the uncertainty in the ^{56}Fe g-factor used to calibrate the TF, namely, $g(2_1^+;^{56}Fe) = 0.61\pm0.08$[25].

As the g-factor obtained agrees with the empirical $f_{7/2}$ shell model value of 1.456 [2] and with the measured [11] g-factor of the 2_1^+ state of ^{54}Fe [also a $(\pi f_{7/2})^n$ configuration], the assumptions involved in extracting it from the precession data seem vindicated sufficiently that the measured value of $g(2_1^+;^{52}Cr)$ be used with confidence in the following analysis.

5.2 High Velocity TF Strengths for ^{52}Cr in Fe

Average TF strengths derived from the measured TF precessions for high velocity ^{52}Cr ions traversing Fe hosts are presented in table 4. The average TF strength (in Tesla) is given by

$$\langle B\rangle = 0.0209\phi/\tau[1-e^{-t_{fe}/\tau}], \qquad (3)$$

where t_{fe} is the mean transit time through the Fe foil and ϕ is the observed precession $\phi = \Delta\theta/g$ in milliradians. The average ion velocity within the ferromagnetic host, $\langle v/v_o\rangle$ was calculated from the reaction kinematics and measured target layer thicknesses using stopping powers from ref. [26]:

$$\langle v/v_o \rangle = \int_o^{t_{Fe}} (v/v_o) e^{-t/\tau} (dt/\tau) \left[1 - e^{-t_{Fe}/\tau}\right]^{-1} \qquad (4)$$

Table 4 also presents a comparison between the present measured TF precessions and those predicted by the three TF parametrizations for Fe hosts which follow:

(i)"Rutgers" [21]

$$B_{RU} = 16.9\ Z^{1.1}\ (v/v_o)^{0.45}\ \text{Tesla} \qquad (5)$$

(ii) "Chalk River" [1]

$$B_{CR} = 19.0\ Z\ (v/v_o) e^{-0.12(v/v_o)}\ \text{Tesla} \qquad (6)$$

(iii) Present (derived in section 7.4)

$$B_P = a\ Z(v/v_o) \left[1 + e^{(7-v)/\sigma v_o}\right]^{-1} \text{Tesla} \qquad (7)$$

where for $\sigma = 2$, $a = 12.6$ (PAR1) and for $\sigma = 3$, $a = 13.5$ (PAR2).

6. Interpretation

6.1 Comparison with Transient Field Parametrizations

In fig 6 our measured average TF strengths for ^{52}Cr (displayed in table 4) are plotted as a function of ion velocity along with the TF parametrizations. To compare the Fe and Cr results in a single figure,

the field strengths for Fe are divided by 26/24. It is apparent from both table 4 and fig 6 that the observed strength for Cr<u>Fe</u> at velocities above $8v_o$ is significantly lower than values predicted by the Rutgers [21] and Chalk River [1] parametrizations. It is also seen from table 4 and fig. 6 that both parametrizations of the form of eq (7) describe the higher velocity data well, with the fit from PAR2 being slightly better (although the errors are too large to make a distinction). The velocity-dependence of the field strength is similar to that found for rare-earth ions; the Chalk River form [eq (6)] can be brought into fair accord with the data in table 4 if its multiplicative constant is reduced from 19.0 to 14.2.

6.2 Comparison with Polarized Electron Capture Model.

In the polarized electron capture model of the TF as presented by Eberhardt et al [13,27], the TF strength is written in terms of the contact fields B_{ns} at the nucleus resulting from unpaired s-electrons of the ion:

$$B_{tr}(v) = \sum_n \xi_{ns}\ (v) F_1^{ns}(v) B_{ns}\,, \qquad (8)$$

where F_1^{ns} is the (velocity-dependent) fraction of single vacancies in the ns electron orbital, and ξ_{ns} is the degree of polarization of these vacancies. Table 5 shows calculated contact fields at the Cr nucleus from single ns vacancies, together with neutral-atom and hydrogenic atom electron velocities for these orbitals, v_{ns}. Using the condition $F_1^{ns}(v_{ns}) \sim 0.5$ [27], the contribution of 2s vacancies to the TF strength at $v \sim 8v_o$ is $B_{2s}(8v_o) = 10.4\xi_{2s}$ kTesla. Taking $\xi_{2s} = 0.13$ as evidenced for K-vacancies of ions of $Z \sim 8$ at somewhat lower ion velocities

[13,14,18] gives a 2s contribution to the TF strength of 1.35 kT which is about a factor of 1.6 greater than the total field strength observed (table 4). As well as this 2s component, there will also be a 1s contribution to the total TF stength at Cr velocities of ~ $8v_o$. Although the relative magnitudes of 1s and 2s contributions are not determined at present, the measured field strength sets a conservative limit on the 2s polarization degree: $\xi_{2s}(8v_o)<0.08\pm0.02$.

As the product $F^{1s}(v)B_{1s}$ in eq (8) is certainly expected to <u>increase</u> monotonically with increasing velocity up to ~ $24v_o$ [13], our observation that the Cr<u>Fe</u> TF strength does not increase with increasing velocity between $8v_o$ and $12v_o$ must be attributed to a fall in the K-shell polarization degree ξ_{1s} in this velocity regime. It is worth noting that K-vacancy fractions for Si ions traversing Ni hosts at v ~ $7v_o$ ($Zv_o/2$ for Si) have been measured to be $F_1^{1s}(Zv_o/2)$ ~ 0.2 [29]. If this value were extrapolated to Cr ions moving at ~$12v_o$ ($Zv_o/2$ for Cr), and a polarization degree of ξ_{1s} = 0.13 assumed, a TF strength of ~6kT would result. In contrast, the present measured field strength is less than one sixth of this value, suggesting a lower polarization, $\xi_{1s}(11v_o)$ ~ 0.02 ± 0.01.

7. Discussion

On the basis that polarization-transfer mechanisms are responsible for the decrease of the TF with increasing velocities significantly below Zv_o, we attempt to develop an understanding of such phenomenona in this section. We first review a specific two-step polarization transfer mechanism proposed earlier [13,14,28,29]; then we outline a possible interpretation of the apparent reduction in inner-shell polarization at ion velocities above ~ $8v_o$.

7.1 Two-Step Polarization Transfer

In figure 7 a simplified representation of the two- step polarization transfer mechanism proposed by Dybdal et al [29] is presented for the case of oxygen in iron. Relative order of magnitude estimates of relevant electron-capture and -loss cross-sections are indicated. Electron-capture cross-sections were estimated using the Brinkmann-Kramers (BK) formula [30]. In the two-step mechanism proposed, polarized electrons are initially captured into the outer shells of the moving ion, then polarization is transferred to the inner shells by spin-dependent transitions, etc. This two-step model rests on two observations: First, that the K-vacancy polarization degree inferred for low-velocity O and F ions in Fe is ~ 0.13, which is effectively the polarization degee of the outershells of the Fe host. Second, that the BK formula predicts that these moving ions predominantly capture polarized electrons from the M-shell of Fe into their L-shells.

However, the assumption that the BK formula gives a reliable indication of electron-capture cross-section trends for low-velocity ions traversing a solid must be questioned. Strictly, the BK cross-section applies for electron capture from occupied host shells to an initially bare ion [30]. As it relates to the TF phenomenon for intermediate mass ions, this approximates the real situation only for $v \gtrsim Zv_o/2$. Furthermore, the BK approach does not take into account possible distortions of the projectile and host orbitals during the collision. As it is well established [13,14] that molecular orbital (MO) mechanisms are of critical importance for producing projectile inner-vacancies at low collision velocities, it might be expected that MO distortion of the atomic orbitals during collisions plays a vital role in the means by which polarization is transferred to inner vacancies of the ion. Indeed, the

observation of comparable TF precessions for ^{12}C ions in Fe and Ni hosts has been attributed to direct K-shell polarization of C via promotion in the 3dσ MO at velocities somewhat lower (~$2v_o$) than those considered here [31]. At the higher ion velocities of present interest direct polarization within the 3dσ MO is not possible; yet a less direct, but nevertheless critical, role is still likely to be played by MO mechanisms [30].

Another difficulty with the two-step mechanism as previously formulated is that it relies on polarization being "stored" in the outer shells of the moving ion; it predicts therefore [13] a diminution of the TF strength when the outer electrons are stripped off the ion, i.e., when the ion velocity exceeds the outer-electron velocity. For oxygen ions this velocity would be $v \gtrsim Zv_o/2 = 4v_o$. Yet, Becker et al [28] have observed an undiminished polarization degree of 0.13 for K-vacancies of oxygen ions moving at velocities up to ~ $8v_o$. Their result implies an effectively direct transfer of host polarization to the K-shell of oxygen, at least for ion velocities between $4v_o$ and $8v_o$. While not excluding the possibility of a two-step transfer via the outer orbitals of the ions at lower velocities, these experimental data make it reasonable to ask whether another means of polarization transfer may pertain even for oxygen velocities below $4v_o$.

7.2 Polarization Transfer $2v_o \leq v \leq 7v_o$

Molecular-orbital correlation diagrams were constructed according to the rules of Eichler et al [32] for various ions of atomic number between 8 and 30, in Fe hosts. As an example, fig 8 shows MO correlation diagram for O + Fe and Si + Fe. For $Z<9$ (e.g., oxygen) it is found that during collisions the K- and L- shells of Fe become more tightly bound

(connecting with the united atom (UA) K- and L- orbitals) while the projectile K-shell becomes less bound. These trends may mediate a "quasi-direct" transfer of M-shell polarization into K-shell vacancies of the ion: during the collision the unpolarized K- and L- shells of Fe become energy mis-matched with the projectile K- shell, while the projectile K-shell becomes more energy-matched with the polarized M-shell of Fe. For Z>9 the couplings of the Fe L-shell are not as straightforward; the 2p orbital couples to the UA L-shell, but the 2s orbital is promoted. However, the projectile 2s-orbital which produces most of the TF strength for these ions is even more strongly promoted.

For all cases there appear complex connections and crossings of the "TF active" projectile orbitals with orbitals connecting to the M- shell of Fe in the separated-atom limit. In view of this, an effective mixing of electrons in the projectile "TF-active" orbitals with those of the polarized M-shell of Fe might be expected during the collisions. The inner-vacancy polarization would then be close to the average polarization of the Fe M-shell, as is indeed observed for O in Fe [13,14,28]. An analogous picture for inner-vacancy production in collisions of ions of large atomic number, in which very complex and densely spaced level crossings are treated in a statistical approach under dynamic conditions, has been discussed by Brandt and Jones [33]. We suggest that, for moderate ion velocities ($2v_o < v <$ Fe L-shell velocity i.e. $\sim 7v_o$), the MO mechanisms may provide a means by which host polarization is transferred 'directly' into inner shells of the ion. At higher velocities, beyond about $7v_o$, the MO adjustment of the Fe L-shell cannot take place during the collisions. This situation is considered in the next section.

7.3 Polarization Transfer at ion velocities above ~$7v_o$

For ions of $8<Z<30$ traversing Fe hosts at velocities higher than ~$7v_o$, the BK approach to electron capture becomes appropriate. The BK calculations for these higher velocity projectiles indicate that almost all of the electron capture to the ion (primarily to inner-shells) takes place from the unpolarized Fe L-shell. This would imply for $v \gg 7v_o$ that the polarization degree of any orbital of the ion must be much smaller than 0.13. It would seem then, that a diminution of the TF must begin at a critical velocity smaller than Zv_o for ions of $Z>8$. If this picture were correct, the critical velocity would correspond to those ion velocities for which appropriate MO adjustments can no longer occur. For Fe hosts, this is around $7v_o$ above which MO effects are no longer applicable for the Fe L-shell. As the ion velocity increases beyond $7v_o$, unpolarised L-shell electrons are almost exclusively captured by the moving ion, and the polarization of inner-vacancies must therefore diminish and so too the TF strength.

7.4 A Model-Based Parametrization.

To date most forms adopted for transient-field parametrizations have been chosen on empirical grounds alone. Here we attempt to fit the high-velocity Cr data with a simple model-based parametrization. For simplicity it is assumed that the polarization of all shells of the ion is the same. Although this will not be true strictly, it is a reasonable approximation since one s-orbital of the ion usually dominates the TF strength at a given ion velocity. Eq (8) may then be rewritten

$$B_{tr}(v) \sim \xi(v) \sum_n F_1^{ns}(v) B_{ns} \qquad (9)$$

Our qualitative arguments above suggest a polarization degree $\xi \sim 0.13$ at

low velocities ($v \lesssim 7v_o$); $\xi \sim 0$ at high velocities ($v >> \sim 7v_o$) and for Fe hosts, $v=v_o \sim 7v_o$ is the change-over point. We therefore parametrize the velocity dependence of the polarization transfer as a Fermi function:

$$\xi(v/v_o) = 0.13 \left[1 + e^{-(v_o - v)/\sigma v_o} \right]^{-1} \qquad (10)$$

where we expect $\sigma \sim 2$ (estimated from measurements of Becker et al [28]). For further simplicity, we assume

$$\Sigma F_1^{ns}(v/v_o) B_{ns} \sim C\, Z(v/v_o)^p \ , \qquad (11)$$

and for Cr and Fe in Fe we take, as a reasonable approximation, p=1; from the B_{ns} values of table 5 and expected vacancy fractions of 0.5 at $v = v_{ns}$, we anticipate $50 \lesssim C \lesssim 200$ Tesla.

Our model-based parametrization therefore takes the form of eq. (7) above (where $a = 0.13C$). The TF data for Fe<u>Fe</u> and Cr<u>Fe</u> were fitted for $\sigma=2$ and $\sigma=3$ (only points for $\langle v \rangle \gtrsim 5\ v_o$ were included). As the value of the parameter σ is not well defined by the present data, the parameter C alone was varied, yielding best fit values of C=96.9 Tesla ($\sigma=2$) and C = 104 Tesla ($\sigma=3$) [cf. eq (7)]. The results of these fits are compared with the data in fig 6.

7.5 Comparison with Heavy Ion Results

For rare-earth ions (particularly ^{169}Tm, ^{156}Dy) traversing Fe foils with velocities between 1.5 v_o and 10.5v_o, the Chalk River group [1] has obtained transient field strengths well described by eq (6). They observe that the TF becomes nearly constant with velocity for $v \gtrsim 7v_o$. The

present results for Cr in Fe show a similar levelling of the TF strength with velocity for $v \gtrsim 7v_o$. Indeed, the parametrization of eq. (7), when fitted to the TF data reported in ref [1] by the Chalk River group, yielded a good fit with a=16.2 Tesla for σ=3.

Unfortanately, neither the rare-earth nor the Cr results are sensitive to the choice of the parameter σ. Yet some Z-dependence of this parameter should be expected. Bell and Betz [34] have explained observed oscillatory yields of K x-rays from 120 MeV ^{35}Cl ions traversing various target media in terms of velocity-matching effects in the Brinkmann-Kramers electron-capture cross section. Such an effect, if present in TF studies, could be manifest as a Z-dependent variation of the parameter σ in eq. (10).

Finally, the Chalk River group has observed and discussed the diminution of TF strengths for high-velocity Pb ions traversing Gd hosts [35,36], and they attribute the diminishing TF strength to a less effective polarization transfer at high ion velocities. However, their approach retains the two-step process. Assuming that host polarization is effectively transferred to (and stored in) the outer orbitals of the ion, and that the polarization of a given orbital is independent of ion velocity, the observed reduction in TF strength with increasing velocity was attributed by them to a diminished transfer of outer-shell polarization to the deeper s- orbitals which produce the TF at high velocities. In contrast, our approach has been (i) to question the validity of a two-step framework proceeding via outer orbitals of the ion, particularly at high velocities, and (ii) to suggest that the TF strength does not increase at high velocity simply because the rapidly-moving ions tend not to interact with the slow-moving polarized electrons of the ferromagnet.

8. Conclusion

The g-factor of the 2_1^+ state of ^{52}Cr has been measured to be g=1.50±0.25, in good accord with the empirical $f_{7/2}$ shell model value of 1.456 [2]. We have also measured TF strengths for ^{52}Cr ions traversing polarized Fe hosts at velocities up to ~12v_o to be somewhat lower than the predictions of previous parametrizations. The observed field strengths have been discussed in terms of possible polarization-transfer mechanisms. It has been suggested that the TF for Fe hosts may diminish in general for ion velocities above about 7v_o, and that the velocity-dependence of this diminution may be sensitive to atomic-number dependent aspects of electron-capture cross sections. While the ion-solid interaction aspect may prove an interesting area for future research, further charting of high-velocity transient field strengths will become necessary if the TF is to be expolited to measure g-factors of nuclear states with ions recoiling at these high velocities.

Acknowledgements

The authors sincerely appreciate the co-operation and suport of the staff of the Australian National University 14UD Pelletron Laboratory. Dr J. Gerl and Mr S.J. Poletti are thanked for help with collection of experimental data, as are Mr B. Szymanski and Mr A.H.F. Muggleton for their technical support. The interest shown in aspects of this work by Dr P.B. Treacy is gratefully acknowledged. One of us (C.E.D) acknowledges the support of a Melbourne University Research Grant. This research was supported, in part, by grants from the Australian Research Grants Scheme and Budget Rent-a-Car (Australia).

References

[1] H.R. Andrews, O. Häusser, D. Ward, P. Taras, R. Nicole, J. Keinonen, P. Skensved and B. Haas, Nucl. Phys. A383(1982)509;
O. Häusser, in High Angular Momentum Properties of Nuclei, ed. N.R. Johnson (Harwood academic, Chur, 1983) p125.

[2] W. Kutschera, B.A. Brown and K. Ogawa, Revista Del Nuovo Cimento 1(1978)49.

[3] A. Winther and J. de Boer, Coulomb excitation, ed. K. Alder and A. Winther (Academic, New York 1966) p303.

[4] K.S.Krane, Nucl. Inst. Meth., 98(1972)205;
K.S. Krane, Nucl. Inst. Meth. 109(1973)401.

[5] M.J.L. Yates, in α, β, γ Ray Spectroscopy, ed. K. Siegbahn (North-Holland, Amsterdam, 1968) Vol 2, p. 1691.

[6] A.E. Stuchbery, H.H. Bolotin, C.E. Doran and A.P. Byrne, Z. Phys. A322(1985)287;
A.E. Stuchbery, H.H. Bolotin, C.E. Doran, I. Morrison, L.D. Wood and H. Yamada, Z. Phys. A320(1985)669;
L.D. Wood, H.H. Bolotin, I. Morrison, R.A. Bark, H. Yamada and A.E. Stuchbery, Nucl. Phys. A427(1984)639;
A.E. Stuchbery, L.D. Wood, R.A. Bark and H.H. Bolotin, Hyp. Int. 20(1984)119;
H.H. Bolotin, I. Morrison, C.G. Ryan, and A.E. Stuchbery, Nuc. Phys. A401(1983)175.

[7] A.E. Stuchbery, I. Morrison, L.D. Wood, R.A. Bark, H. Yamada and H.H. Bolotin, Nucl. Phys. A435(1985)635.

[8] P.M.S. Lesser, D. Cline, P. Goode and R.N. Horoshko, Nucl Phys. A190(1972)579.

[9] A. Abragam and R.V. Pound, Phys. Rev. 92(1953)943.

[10] K.S. Krane, Hyp. Int. 15/16(1983)1069.

[11] J.M. Brennan, N. Benczer-Koller, M. Hass and H.T. King, Phys. Rev. C16(1977)899.

[12] N.K.B. Shu, R. Levy, N. Tsoupas, W. Andrejtscheff, A. Lopez-Garcia, A.E. Stuchbery, H.H. Bolotin and N. Benczer-Koller, Hyp. Int.9(1981)65.

[13] K. Dybdal, J.S. Forster and N. Rud, Nucl. Inst. Meth. 170(1980)233.

[14] K. Dybdal, J.S. Forster and N. Rud, Phys. Rev. Lett 43(1979)1711.

[15] A.E. Stuchbery, L.D. Wood, R.A. Bark and H.H. Bolotin, Hyp. Int 20(1984)119.

[16] A.E. Stuchbery, C.G. Ryan and H.H. Bolotin, Hyp Int. 13(1983)275.

[17] A.E. Stuchbery, Ph.D. thesis, University of Melbourne, (unpublished).

[18] A.E. Stuchbery, H.H. Bolotin and C.E. Doran, submitted to Hyperfine Interactions.

[19] A.E. Stuchbery, H.H. Bolotin, A.P. Byrne, C.E. Doran and G.J. Lampard, to be published.

[20] M. Hass, J.M. Brennan, H.T. King, T.K. Saylor and R. Kalish, Phys. Rev. C14(1976)2119.

[21] N.K.B. Shu, D. Melnik, J.M. Brennan, W. Semmler and N. Benczer-Koller Phys. Rev. C21(1980)1828.

[22] C.E. Violet and D.N. Pipkorn, J. App. Phys. 42(1971)4339.

[23] J.L. Eberhardt and K. Dybdal, Hyp. Int 7(1980)387.

[24] G.K. Hubler, H.W. Kugel and D.E. Murnick, Phys. Rev. C9(1974)1954; R.R. Borchers, G.M. Heestand, H.W. Kugel and R. Kalish, in Nuclear Reactions induced by Heavy Ions, eds. R. Bock and W.R. Hering, (North-Holland, Amsterdam, 1970) p.415.

[25] Table of Isotopes, 7th ed., eds. C.M. Lederer and V.S. Shirley (Wiley, New York, 1978) app. VII.

[26] J.F. Ziegler, App. Phys. Lett. 31(1977)544.

[27] J.L. Eberhardt, R.E. Horstman, P.C. Zalm, H.A. Doubt and G. Van Middelkoop, Hyp. Int 3(1977)195.

[28] A. Becker, A. Holthuizen, A.J. Rutten, C.P.M. van Engelen and G. van Middelkoop, Hyp. Int.11(1981)279.

[29] K. Dybdal, J.L. Eberhardt and N. Rud, Phys. Rev. Lett 43(1979)592.

[30] H.-D. Betz, in Atomic Physics in Nuclear Experiments, eds. B. Rosner and R. Kalish (Adam Hilger, Bristol, 1977) p 255;
H.C. Brinkmann and H.A. Kramers, Proc. Acad. Sci. Amsterdam 33(1930)973.

[31] K.-H. Speidel, G.J. Kumbartzki, W. Knauer, G. Krösing, V. Mertens, P.N. Tandon, J. Gerber, R.M. Freeman and M.B. Goldberg, Phys. Lett 76A(1980)414.

[32] J. Eichler, U. Wille, B. Fastrup and K. Taulbjerg, Phys. Rev.A14(1976)707.

[33] W. Brandt and K.W. Jones Phys. Lett. 57A(1976)35.

[34] P. Bell and H.-D. Betz, J. Phys. B: Atom Molec. Phys. 10(1977)483.

[35] O. Häusser, H.R. Andrews, D. Ward, N. Rud, P. Taras, R. Nicole, J. Keinonen, P. Skensved and C.V. Stager, Nucl. Phys. A406(1983)339.

[36] O. Häusser, H.R.Andrews, D. Horn, M.A. Lone, P. Taras, P. Skensved, R.M. Diamond, M.A. Delepanque, E.L. Dines, A.O. Macchiavelli and F.S. Stephens, Nucl. Phys. A412(1984)141.

TABLE 1. Experimental Details and Results for ^{52}Cr and ^{56}Fe

Beam		Target		L_{Fe} [a]	T_{Fe} [b]	E_i [b]	v_i/v_o [b]	E_e [b]	v_e/v_o [b]	$\langle v/v_o \rangle$ [b]	$\Delta\theta$ [c]
Ion	Energy (MeV)	Number	Ion	(μm)	(ps)	(MeV)		(MeV)			(mrad)
^{81}Br	220	I	^{52}Cr	10.7	0.61	183	11.7	24	4.2	8.4	-28 ±7
^{81}Br	230	II	^{52}Cr	5.7	0.24	197	12.1	113	9.2	10.9	-12 ±7
^{16}O	36	II	^{52}Cr	5.7	0.94	20 [d]	4.0	0	0	1.65	-24.6±3.8
		II	^{52}Cr	5.7	0.86	14 [d]	3.3	0	0	1.40	-20.7±3.2
^{16}O	35	II	^{56}Fe	5.7	0.95	21	3.9	0	0	1.53	- 5.7±0.7

a) Measured thickness of Fe foil.

b) Transit time of target ions through Fe foils, T_{Fe}, energies (velocities) of ions incident upon, $E_i(v_i/v_o)$, and emergent from, $E_e(v_e/v_o)$, the Fe foil, and the mean velocity of the ions in the Fe foil, $\langle v/v_o \rangle$, were obtained using the measured target and Fe foil thicknesses, the reaction kinematics, and the stopping powers of ref.[26]. Bohr velocity $v_o = c/137$.

c) Measured precession angle including transient field precession and, for measurements employing ^{16}O beams, static-field precession.

d) Velocities of Cr ions incident upon Fe layer selected by window on backscattered particle spectrum; see fig. 4 and text.

TABLE 2. Static Field Interactions for ^{188,190,192}Os in Fe Foils

Isotope[a]	Measured Static Field Strength[b] (Tesla)	
	Target I	Target II
^{188}Os g=0.292±0.010 τ=1025 ps	-107^{+11}_{-15}	-96^{+5}_{-10}
^{190}Os g=0.350±0.011 τ= 528 ps	-102^{+6}_{-7}	-102±6
^{192}Os g=0.396±0.010 τ= 417 ps	-109±5	-114±5
Average	<-106±4>	<-106±4>

a) Gyromagnetic ratios from ref.[7]; mean lives from ref.[25].

b) Uncertainties quoted do not include relatively small errors in previously measured mean lives.

TABLE 3A. Present and Previous Transient Field Results for ^{56}Fe.

E_i (MeV)	E_e (MeV)	$\phi_{tf}(\times 10^3)$ exp[a]	$\phi_{tf}(\times 10^3)$ Calc.[b]	<B> (kT)	Ref.
21	0	25.1±1.7[c]	25.7	0.55±0.04	present
53	0	36 ±4[c]	36.9	0.60±0.05	[11]
65	21	14.6±2.8	13.9	1.22±0.23	[11-13]
56	31	8.0±1.8	7.7	1.22±0.27	[11-13]
56	14	13.4±2.6	14.9	0.99±0.19	[11-13]

a) $\phi_{tf} = \Delta\theta_{tf}/g$ taking $g(2_1^+;{}^{56}Fe)=0.61\pm0.08$. Errors quoted do not include error in g-value.

b) Transient field precession calculated using eq.(2) of text.

c) Corrected for static field contribution of strength 33.04±0.03 Tesla [10,22]; $\phi_{static} = 15.8$, see text.

TABLE 3B. g-factor results for ^{52}Cr

E_i (MeV)	E_e (MeV)	$\Delta\theta_{exp}$ (mr)	ϕ_{calc} [a] ($\times 10^3$)	$g(2_1^+)$
20	0	-24.6±3.8	-16.68	+1.47±0.23 [b]
14	0	-20.7±3.2	-13.63	1.52±0.23 [b]
				1.50±0.25 [c]

a) Transient- and static-field precession, calculated using eqs.(1) and (2); includes corrections for: decay of ^{52}Cr in target layer before entering Fe foil, decay in flight through Fe foil, and static-field strength of -6.7 Tesla. Uncertainty in ϕ_{calc} is 13.8% (13% uncertainty in previously measured ^{56}Fe g-factor and 4% uncertainty in measured field-calibration precessions, added in quadrature).

b) Statistical error of present precession alone.

c) Error on average g-value includes uncertainties in measured precessions and in field calibration added in quadrature.

TABLE 4. Comparison of Measured and Calculated High-Velocity TF Strengths for ^{52}Cr and ^{56}Fe in Fe

Ion	E_i (MeV)	E_e (MeV)	$\langle v/v_o \rangle$	$\lvert\phi_{exp}\rvert$[a] ($\times 10^3$)	$\lvert\phi_{calc}\rvert$ ($\times 10^3$)				<B> (kT)
					RU[b]	CR[c]	PAR1[d]	PAR2[d]	
^{52}Cr	183	24	8.4	18.7±5.1	31.7	29.6	17.0	20.5	0.85±0.23
^{52}Cr	197	113	10.9	8.0±4.8	16.8	13.8	4.4	7.6	0.78±0.47
^{56}Fe	65	21	5.3	14.6±2.8	15.4	16.4	14.1	13.5	1.22±0.23
	56	31	5.5	8.0±1.8	8.6	9.2	7.9	7.6	1.22±0.27
	56	14	4.7	13.4±2.6	16.5	17.6	15.3	14.5	0.99±0.19

a) ϕ_{exp} inferred from measured precessions using g(Fe) = 0.61 and measured ratio g(Cr)/g(Fe) = 2.46±0.28. Errors quoted for ^{52}Cr precessions include a small contribution from the uncertainty in this ratio.

b) Rutgers parametrization [21]; eq.(5) of text.

c) Chalk River parametrization [1]; eq.(6) of text.

d) Eq.(7) of text with a = 12.6 for σ = 2 (PAR1), and a = 13.5 for σ = 3 (PAR2).

TABLE 5. Contact fields and electron orbital velocities for Cr

Orbital	B_{ns} (kT)	v_{ns}/v_o	
		(neutral)	(hydrogenic)
1s	229	22.9	24.0
2s	20.7	7.9	10.5
3s	2.7	2.6	7.0

Figure Captions

Fig. 1 Measured and calculated (solid curve) γ-ray angular correlations in coincidence with forward-recoiling ^{52}Cr ions, following bombardment of target II with 240 MeV ^{81}Br beams.

Fig. 2 Coincidence spectrum of forward-scattered ions following bombardment of target II with 240 MeV ^{81}Br.

Fig. 3 γ-ray spectrum recorded by an HP Ge detector in coincidence with the particle gate indicated in figure 2.

Fig. 4 Coincidence spectrum of ^{16}O ions backscattered from layered target II.

Fig. 5 Partial γ-ray spectrum recorded in coincidence with beam-ions backscattered from target II. Major lines from Cr and Fe isotopes are labelled. Annihilation rediation (from reactions on light contaminants in the target) is indicated by the symbol γ±.

Fig. 6 Measured transient-field strengths for Fe and Cr ions compared with various parametrizations; see text.

Fig. 7 Representation of two-step polarization transfer as proposed earlier [29] for low-velocity oxygen in iron. Approximate relative magnitudes of some relevant electron transfer paths are shown. Electron-capture cross-sections were estimated using the Brinkmann-Kramers formula [30].

Fig. 8 Qualitative molecular orbital (MO) correlation diagrams for O+Fe and Si+Fe constructed according to the rules of Eichler et al [32].

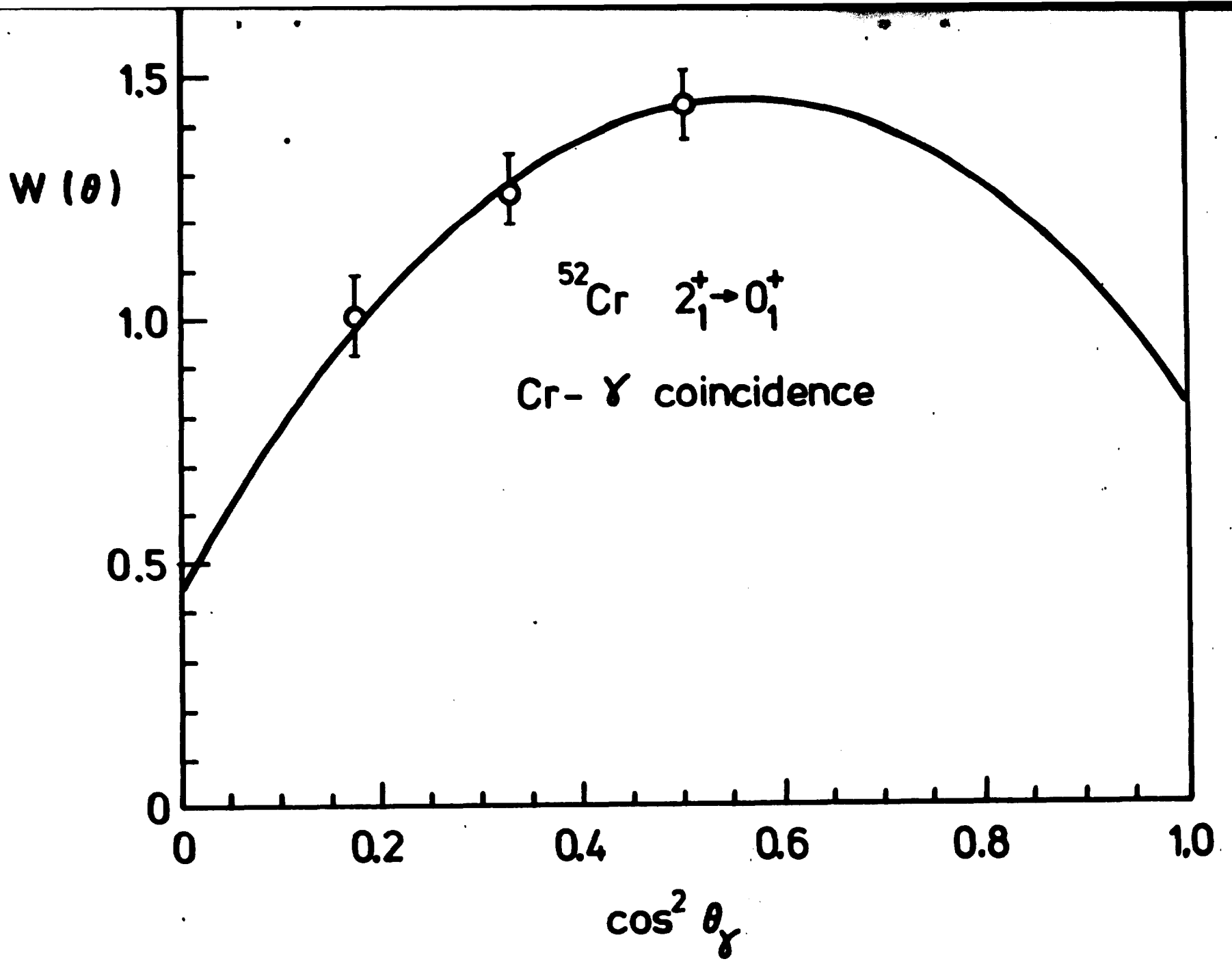
1.5
1.0
0.5
0
W (θ)
^{52}Cr $2_1^+ \rightarrow 0_1^+$
Cr- γ coincidence
0
0.2
0.4
0.6
0.8
1.0
cos^2 θ$_\gamma$

Figure 1

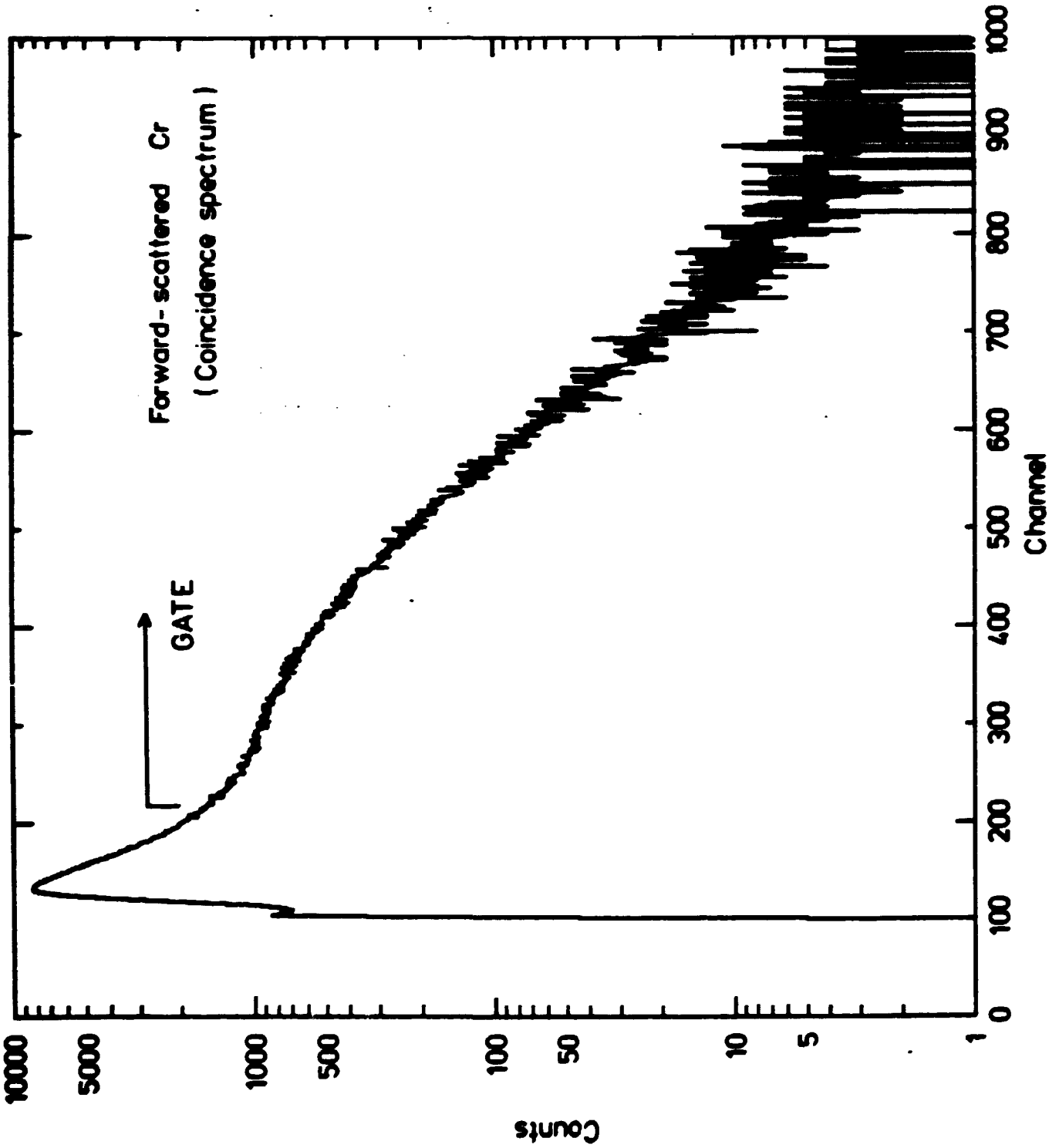
Forward-scattered Cr
(Coincidence spectrum)
GATE
Counts
Channel
10000
5000
1000
500
100
50
10
5
1
0
100
200
300
400
500
600
700
800
900
1000

Figure 2

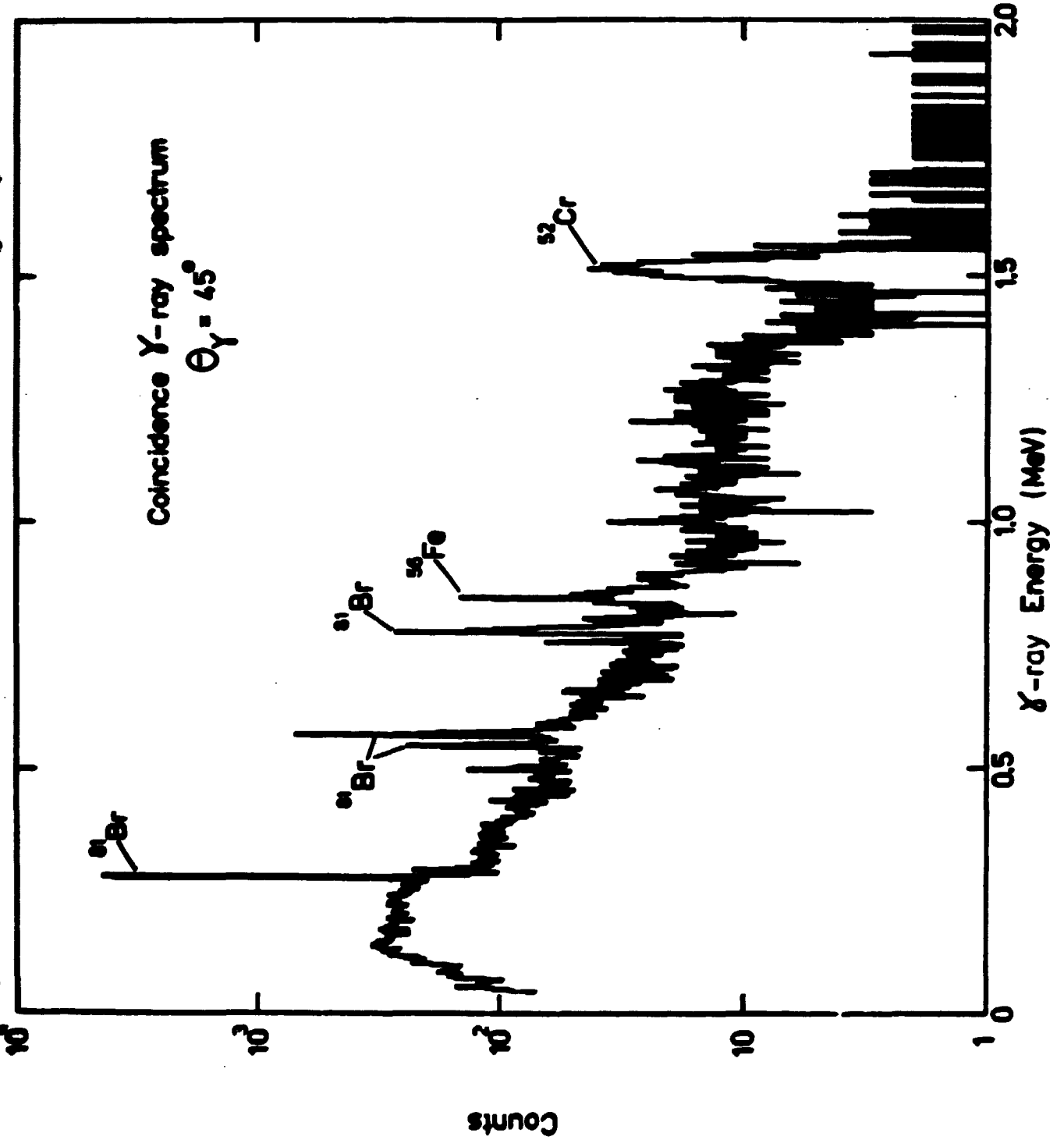
Coincidence γ-ray spectrum
$\theta_\gamma = 45°$
^{81}Br
^{80}Br
^{80}Br
^{81}Br
^{56}Fe
^{52}Cr
Counts
10^4
10^3
10^2
10
1
0
0.5
1.0
1.5
2.0
γ-ray Energy (MeV)

Figure 3

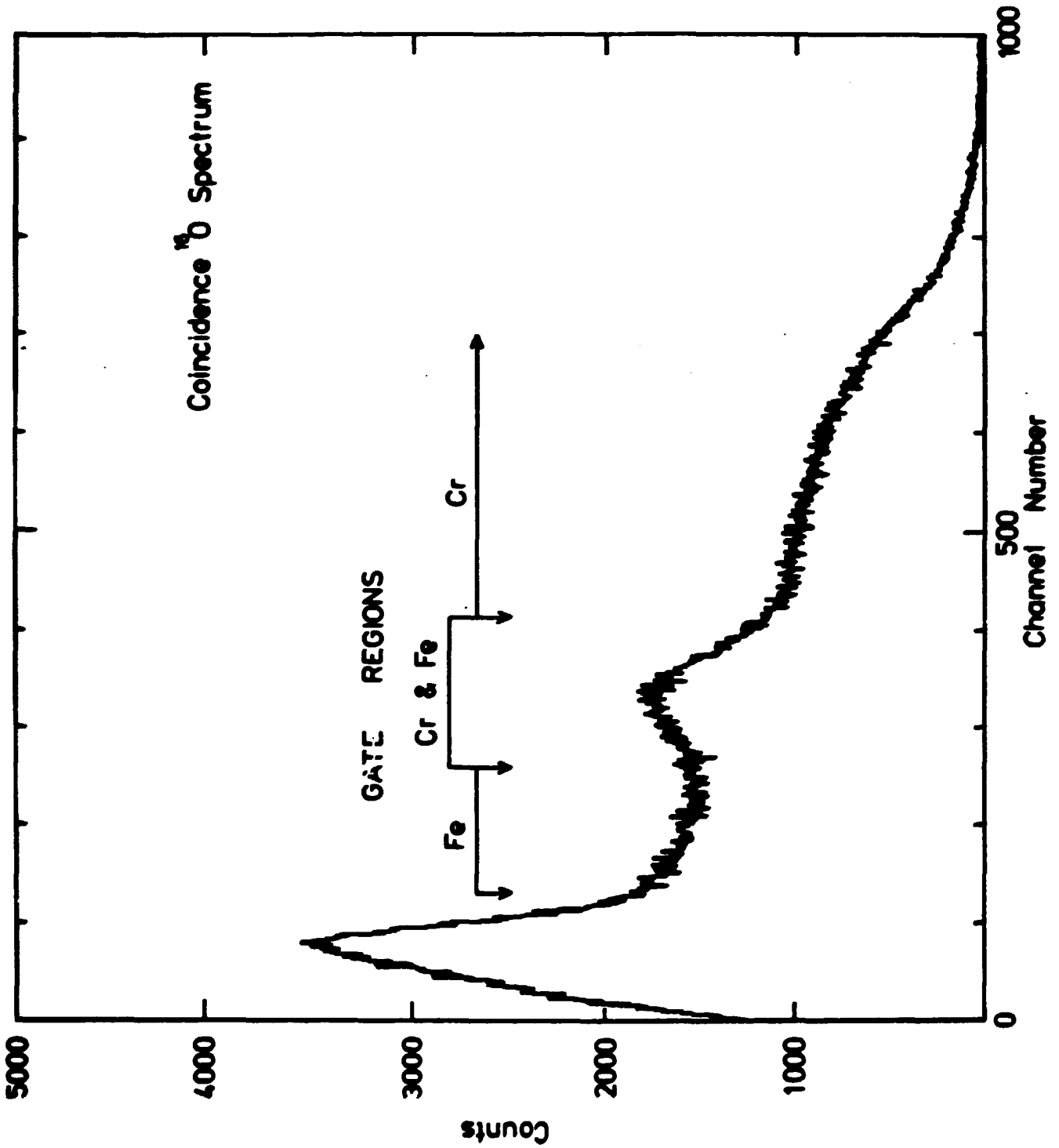
Coincidence ^{56}O Spectrum
GATE REGIONS
Fe
Cr & Fe
Cr
Counts
5000
4000
3000
2000
1000
0
500
1000
Channel Number

Figure 4

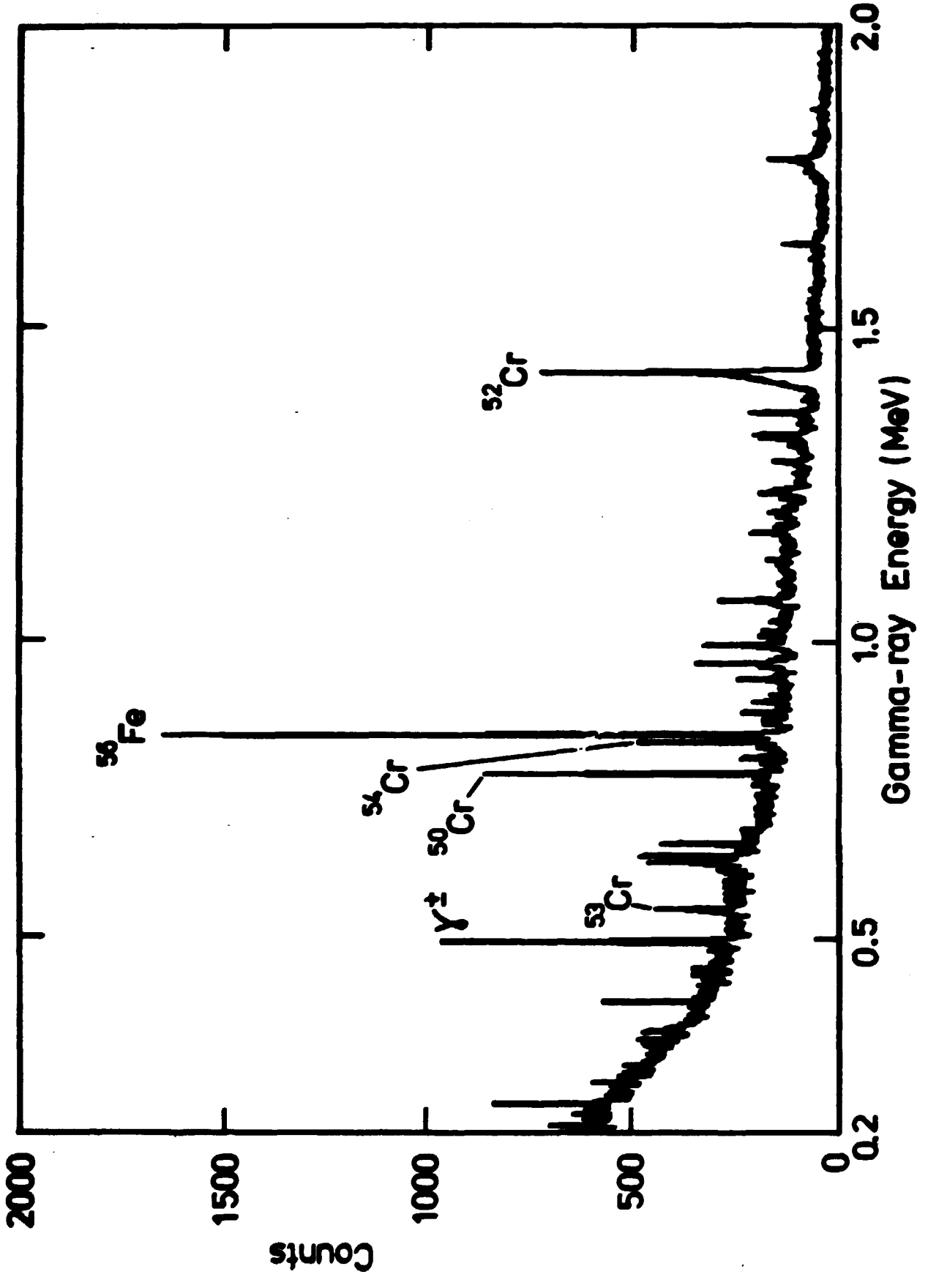
Counts
2000
1500
1000
500
0
0.2
0.5
1.0
1.5
2.0
Gamma-ray Energy (MeV)
56Fe
54Cr
50Cr
Y+
53Cr
52Cr

Figure 5

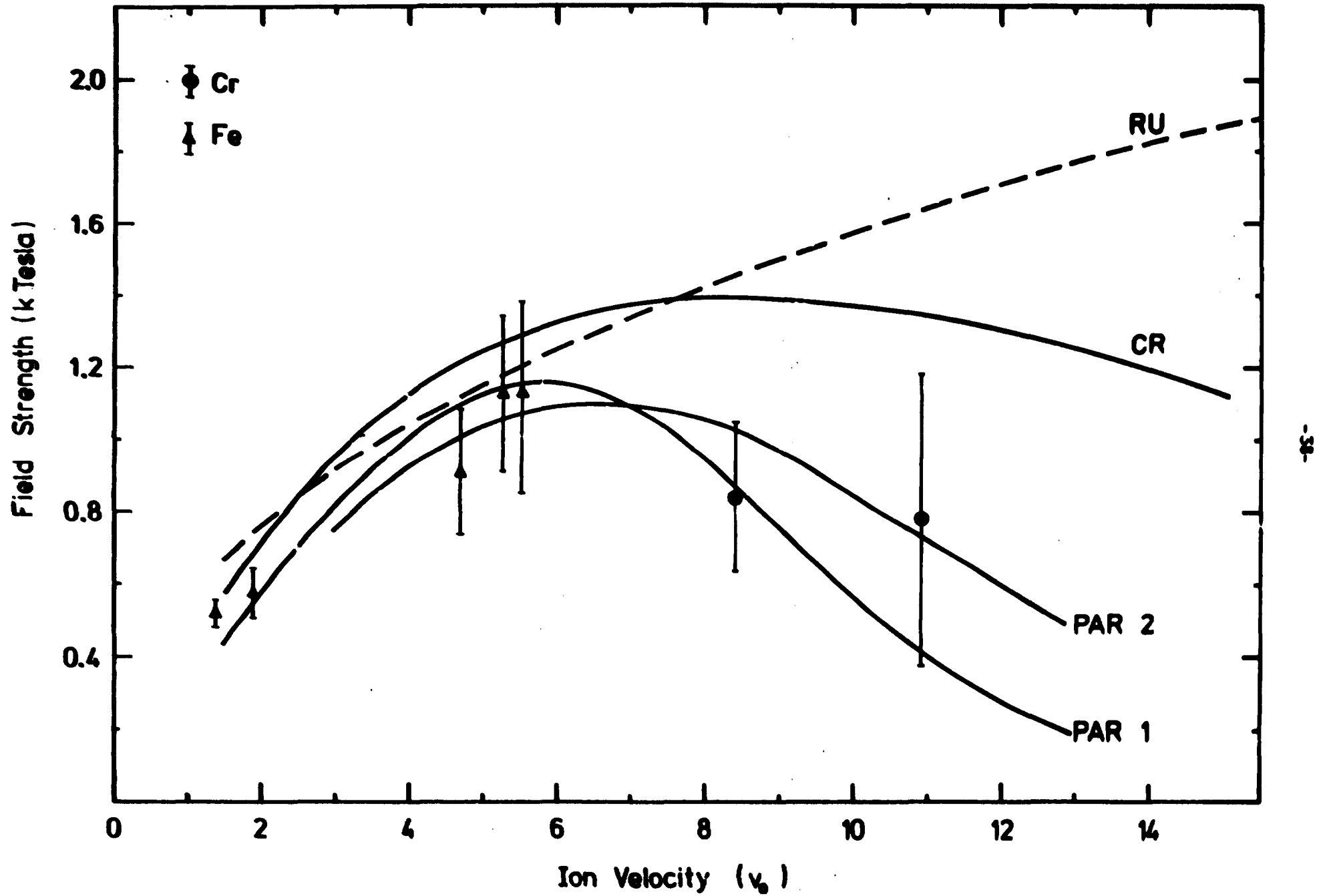
Cr
Fe
RU
CR
PAR 2
PAR 1
Field Strength (k Tesla)
Ion Velocity (v_0)
2.0
1.6
1.2
0.8
0.4
0
2
4
6
8
10
12
14

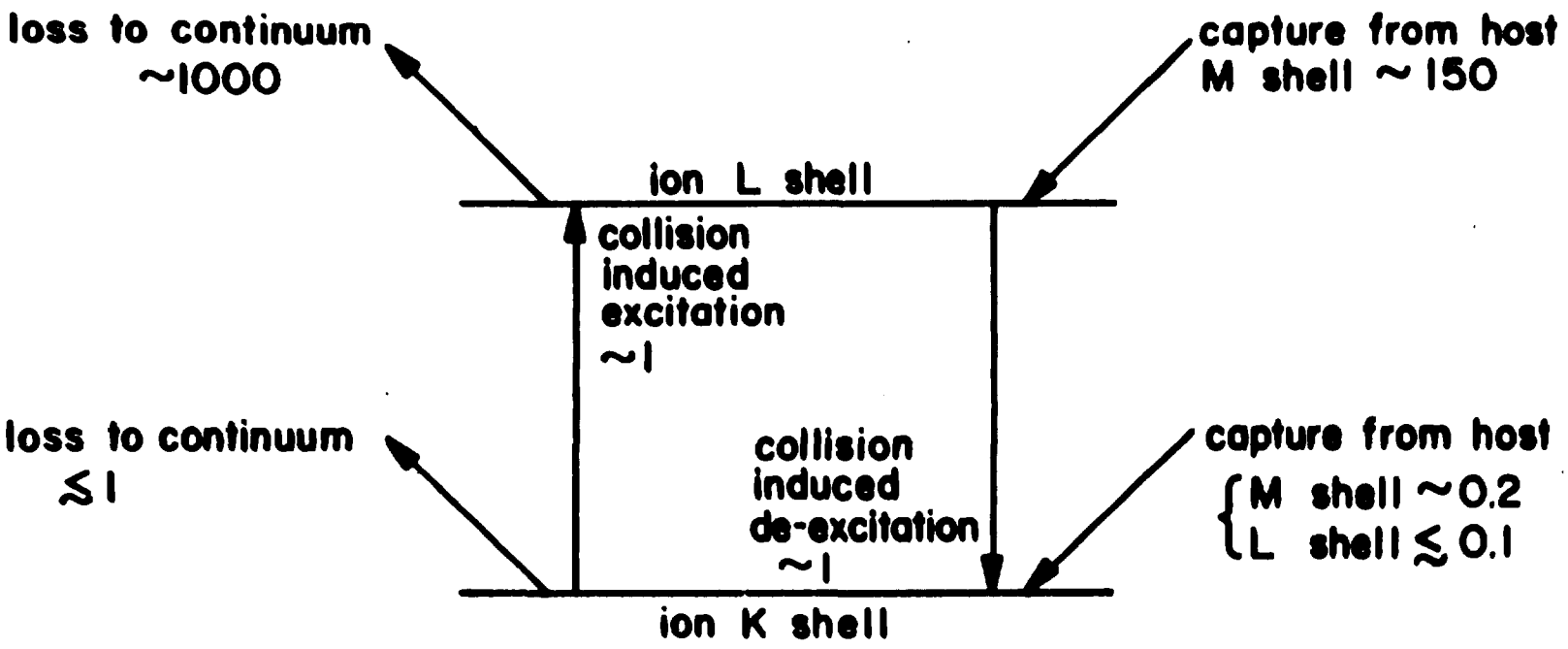
loss to continuum
~1000
capture from host
M shell ~ 150
ion L shell
collision
induced
excitation
~1
loss to continuum
≲1
collision
induced
de-excitation
~1
capture from host
M shell ~0.2
L shell ≲ 0.1
ion K shell

Figure 7

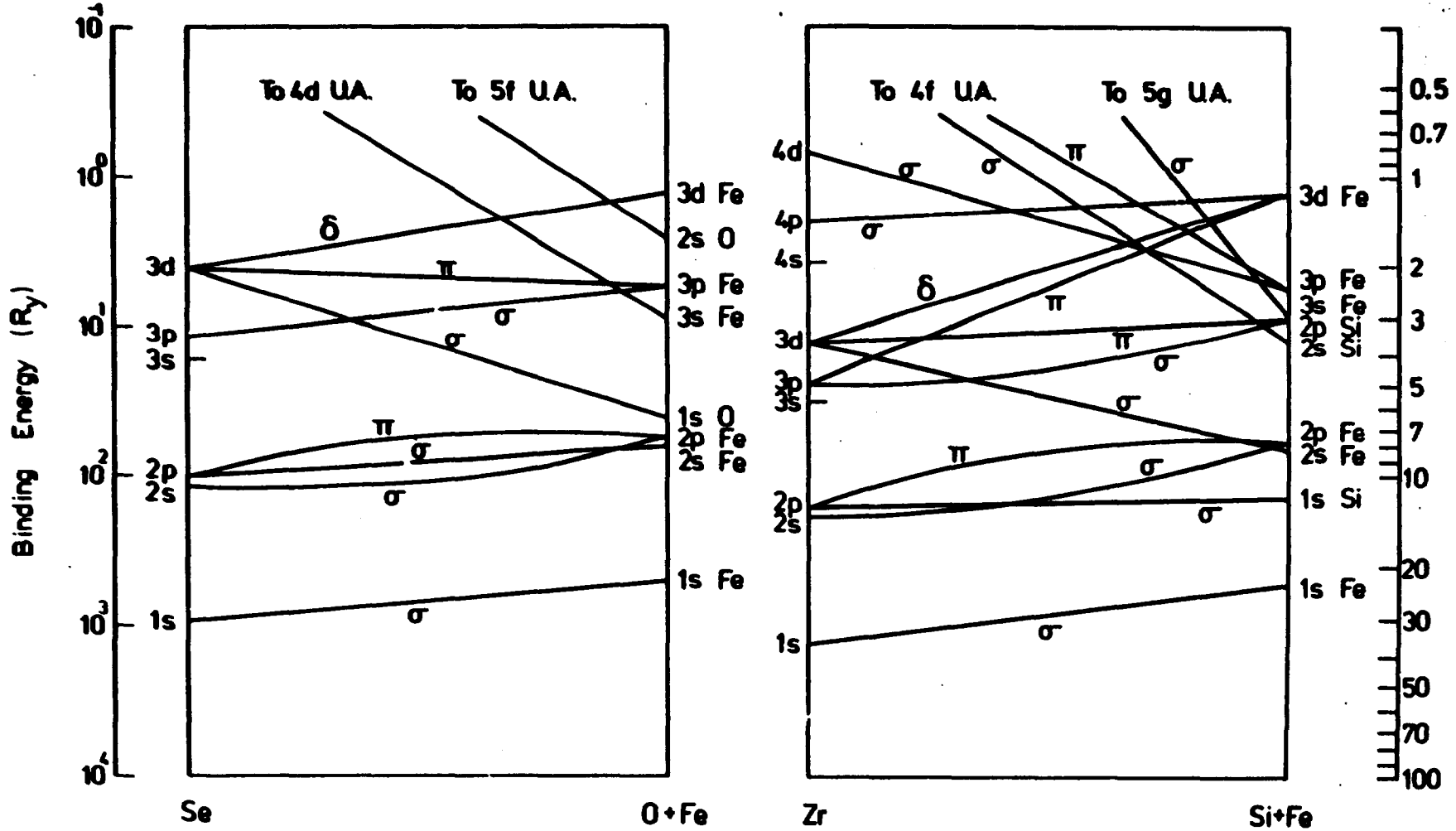
Binding Energy (R_y)
10^1
10^0
10^{-1}
10^{-2}
10^{-3}
10^{-4}
To 4d U.A.
To 5f U.A.
3d
3p
3s
2p
2s
1s
δ
π
σ
3d Fe
2s O
3p Fe
3s Fe
1s O
2p Fe
2s Fe
1s Fe
Se
O+Fe
To 4f U.A.
To 5g U.A.
4d
4p
4s
3d
3p
3s
2p
2s
1s
3d Fe
3p Fe
3s Fe
2p Si
2s Si
2p Fe
2s Fe
1s Si
1s Fe
Zr
Si+Fe
Electron Velocity (V_6)
0.5
0.7
1
2
3
5
7
10
20
30
50
70
100

Figure 8